




**Discovery of topological metamaterials by symmetry relaxation and smooth topological indicators**Cyrill Bösch,<sup>1</sup> Tena Dubček ,<sup>2</sup> Frank Schindler,<sup>3</sup> Andreas Fichtner ,<sup>1</sup> and Marc Serra-Garcia <sup>1</sup><sup>1</sup>*Institute for Geophysics, ETH Zurich, CH-8092 Zurich, Switzerland*<sup>2</sup>*Institute for Theoretical Physics, ETH Zurich, CH-8093 Zurich, Switzerland*<sup>3</sup>*Department of Physics, University of Zurich, Winterthurerstrasse 190, CH-8057 Zurich, Switzerland*

(Received 25 June 2020; revised 30 November 2020; accepted 1 December 2020; published 10 December 2020)

Physical properties of a topological origin are known to be robust against small perturbations. This robustness is both a source of theoretical interest and a driver for technological applications, but presents a challenge when looking for new topological systems: Small perturbations cannot be used to identify the global direction of change in the topological indices. Here, we overcome this limitation by breaking the symmetries protecting the topology. The introduction of symmetry-breaking terms causes the topological indices to become smooth, nonquantized functions of the system parameters, which are amenable to efficient design algorithms based on gradient methods. We demonstrate this capability by designing discrete and continuous phononic systems realizing conventional and higher-order topological insulators.

DOI: [10.1103/PhysRevB.102.241404](https://doi.org/10.1103/PhysRevB.102.241404)

The key idea in topological physics has remained largely unchanged since its beginnings in the explanation of the quantum Hall effect [1] by means of the Chern number [2]: We can associate integer-valued topological invariants to the bulk band properties of a material, and these topological invariants in turn predict the material's boundary physics [3]. A crucial property of topological invariants is that they are insensitive to smooth deformations, as long as these respect the protecting symmetries of the topological invariant [4–6]. This equips topological materials with their characteristic robustness, but presents a challenge from a design point of view, as one cannot systematically discover new topological systems by smoothly modifying a nontopological model in the direction of growth of the topological index. A proof of this challenge is that discovering new topological models is still as much of an art as a science, as exemplified by the diversity of approaches to the design problem. These include engineering the symmetries of the system [7], exhaustive searches of crystal structure databases [8,9], identifying geometries that mimic known topological tight-binding models over a range of frequencies [10,11], using artificial-intelligence constructs such as neural networks [12–14], or optimizing for proxy quantities such as boundary modes [15] or energy transfer [16,17] that, while not topological themselves, are frequently associated with topology.

In this Rapid Communication, we present an approach to the problem of designing topological metamaterials. The proposed approach does not require prior knowledge of the model details, other than the general structure, the relevant invariant, and the protecting symmetries. We start with a parametrized design, which can be a tight-binding model, a unit-cell geometry, or a material property distribution, where some or all of the parameters (e.g., hopping potentials, geometric dimensions, or stiffness values) are allowed to change. We then proceed by relaxing the protecting symmetries [18,19], by allowing symmetry-breaking terms in the model. This has the

effect of lifting the discreteness of the topological invariant. Once the topological invariant becomes a smooth function of the design parameters, we can use small perturbations to determine its direction of change. This allows us to use efficient gradient-based methods to identify the parameter values that produce a topological phase, in which the symmetries are eventually restored.

This Rapid Communication is structured as follows: We will start by describing the approach in the Su-Schrieffer-Heeger (SSH) [20] model, a simple, paradigmatic one-dimensional (1D) lattice model whose topological properties can be characterized by a Berry phase [21]. We will continue by showing that the same idea can be used to design continuous metamaterials, by considering a 1D bar supporting the propagation of elastic waves, but which can nonetheless be described by the same symmetries and topological invariant as the SSH model. Then, we will demonstrate that the proposed approach is general and can be applied to other types of topological invariants besides Berry phases, by considering a double-SSH system whose topology is given by the eigenvalues of the parity operator [22]. Finally, we will show that the proposed approach can be applied beyond conventional topological models, by designing a higher-order topological insulator (HOTI), a recently discovered type of topological system with boundary states more than one dimension below that of the bulk [23,24].

We first illustrate the concept of design by symmetry relaxation using the SSH model [20], which consists of a 1D chain with dimerized hopping potentials of strength  $t$  and  $s$  [Fig. 1(a)]. While the phases of the SSH model are well understood, its simplicity provides a good platform to introduce the gradient-based design approach proposed in this work. The SSH model is described by the Bloch Hamiltonian [20,25,26]

$$H = \begin{pmatrix} 0 & t + se^{ik} \\ t + se^{-ik} & 0 \end{pmatrix}. \quad (1)$$

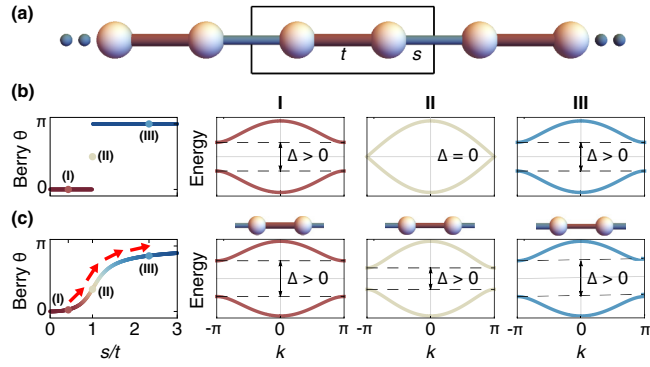


FIG. 1. Symmetry relaxation in the SSH model. (a) Example of an SSH chain. The rectangle highlights the unit cell. The model consists of a dimerized chain with alternating hopping potentials of strength  $t$  and  $s$ . (b) Berry phase (left) and band structure (right) for an SSH chain with intact inversion symmetry, as the hopping  $s$  is varied. (c) Berry phase (left) and unit cell and band structure (right) for an SSH chain with relaxed inversion symmetry, as the hopping  $s$  is varied. The arrows indicate the evolution of a gradient-following optimization of the system parameters.

When the hopping potentials are different ( $t \neq s$ ), the resulting spectrum is gapped. If  $t < s$ , the system is in a topological phase, and finite samples present boundary-localized states in the gap. When  $t > s$ , the system is in a trivial phase, and finite samples do not present in-gap states at the boundary [22,27]. The topology of the SSH model can be characterized by a Berry phase invariant of the form [21,28]

$$\theta = i \oint u^*(k) \frac{d}{dk} u(k) dk, \quad (2)$$

$u(k)$  being the eigenfunction of Eq. (1) with energy below the gap, evaluated at momentum point  $k$ .

Smoothly deforming the system by altering the couplings  $s$  or  $t$  [Fig. 1(b)] does not affect the topological invariant in Eq. (2), unless the system goes through the configuration where  $s = t$ . In this configuration, the lattice is not dimerized, the gap closes, and the topological invariant is not defined. This picture is, however, only true when the symmetry that protects the topological invariant is preserved [22,28,29]—in this case, inversion symmetry. If we eliminate the inversion symmetry, by adding a small scalar potential  $\epsilon \ll |s|, |t|$  acting oppositely on the two sites of the unit cell,

$$H_{\text{relaxed}} = \begin{pmatrix} \epsilon & t + se^{ik} \\ t + se^{-ik} & -\epsilon \end{pmatrix}, \quad (3)$$

we observe two well-understood effects [Fig. 1(c)]: First, the Berry phase changes smoothly when we vary the hopping potentials  $s$  and  $t$ , and second, the gap  $\Delta$  does not close in the configuration where  $s = t$ , meaning that Eq. (2) can be evaluated for all values of the hopping potentials. We refer to such quantities as *smooth topological indicators*. While smooth topological indicators can no longer be interpreted as topological invariants, here we show that they can be a valuable quantity in the process of discovering novel topological systems. In contrast to the invariant in Fig. 1(b), the smooth topological indicator in Fig. 1(c) has a nonzero slope that can

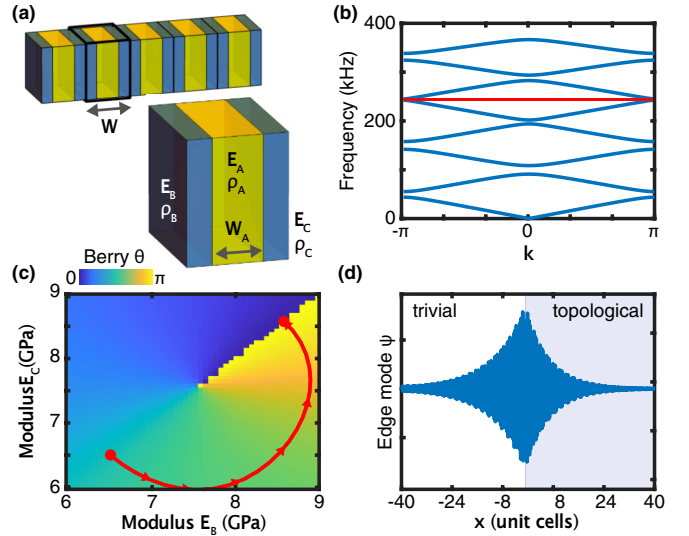


FIG. 2. Design of a phononic topological insulator using smooth topological indicators. (a) Material design made by repeating a three-material unit cell. (b) Dispersion relation for the system in (a). The red region denotes the gap selected for optimization. (c) Multiband Berry phase as a function of the unit cell parameters  $E_B$  and  $E_C$ , while  $E_A$  and  $\rho$  are kept constant. The red line shows a gradient-ascending optimization trajectory starting from a symmetric, trivial phase and ending in a symmetric, topological configuration. (d) Finite element method simulation (COMSOL®Multiphysics) of a localized mode at the interface between two sandwich metamaterials, one topological and one trivial [30], corresponding respectively to the start point and end point in (c). The domain wall is placed at  $x = 0$ , and  $W_A = 0.6759W$ .

be used to determine the direction of parameter change that leads towards the topological phase. The proposed metamaterial design method consists in numerically determining the gradient of the smooth topological indicator, and using it to adjust the model parameters until a topological configuration is reached [30] [Fig. 1(c)].

We will now illustrate the proposed method by designing a continuous phononic metamaterial, whose classical elastic vibration spectrum presents nontrivial band gaps. While the concept of a smooth topological indicator was introduced in the SSH model, a quantum tight-binding model, the Berry phase is a property of the Bloch eigenfunctions and as such can be equally assigned to classical wave propagation problems. In fact, classical systems presenting topological wave phenomena [31–36] are an established platform for the demonstration of novel condensed matter physics: Fragile topological phases [37], higher-order topological insulators [11,38], and Weyl semimetal effects such as axial fields [39] and surface physics [40], were all first observed in classical systems. In contrast to discrete models such as the SSH model, the problem of designing continuous systems with topological wave propagation is not straightforward, due to its higher dimensionality, as both the dynamical variables and material properties are functions of the spatial coordinates.

The continuous phononic metamaterial considered here is a 1D bar of elastic material, made by periodically repeating a unit cell of length  $W$ , consisting of a three-material sandwich

[41,42] with constant density  $\rho$  and elastic moduli  $E_A$ ,  $E_B$ , and  $E_C$  [30], respectively [Fig. 2(a)]. The rod satisfies the elastic wave equation,

$$\rho(x)\partial_{tt}\psi(x,t) + \partial_x[E(x)\partial_x\psi(x,t)] = 0, \quad (4)$$

where  $\psi$  is the displacement along the longitudinal direction ( $x$ ) of the bar,  $\rho$  is the density (assumed uniform throughout the bar), and  $E$  is the elastic modulus. The system presents multiple band gaps [Fig. 2(b)]. To every band gap, we can associate a Berry-phase-like topological invariant, generalized to multiband systems [21],

$$\theta = -i \log \det U, \quad (5)$$

where  $U_{mn} = \langle u_m(-\pi) | e^{-i2\pi x/W} | u_n(\pi) \rangle$ ,  $u_m(k)$ ,  $u_n(k)$  being the Bloch wave functions in the parallel transport gauge [21,30], for all bands  $m, n$  below the band gap under consideration. The topological invariant in Eq. (5), which equals the Berry phase [Eq. (2)] in single-band systems, is protected by inversion symmetry, and becomes a smooth topological indicator when the symmetry is broken by setting  $E_B \neq E_C$ . This is exemplified for the fifth band gap in Fig. 2(c), although the same holds true for all band gaps. Along the line where the  $E_B = E_C$ , inversion symmetry quantizes the Berry phase to the values of 0 or  $\pm\pi$ . However, allowing symmetry violations results in a path through parameter space where the Berry phase transitions smoothly between trivial and topological values, without going through a gap closing. There, a gradient-ascent

algorithm can be used to identify topological configurations of the phononic system in a direct manner. We demonstrate this ability by finding values of  $E_B$  and  $E_C$  resulting in a topological configuration [Fig. 2(c)], and observing the presence of localized modes at the selected band gap in a finite element simulation of the interface between a topological and a trivial metamaterial [Fig. 2(d)]. Two aspects of this result deserve special mention: By having selected realistic initial conditions, we obtain a system geometry and material properties that can be easily realized experimentally. Second, the system ends up naturally in a symmetry-respecting configuration. Symmetry in the final configuration cannot be always guaranteed to appear automatically, but can be restored by penalizing symmetry-breaking terms towards the end of the optimization.

Not all topological insulators can be described by a Berry phase. In the presence of inversion symmetries, an alternative characterization can be established using the eigenvalues [6] of the parity operator, evaluated at inversion-symmetric momentum points in reciprocal space [22]. We will show here that this type of invariant can also be smoothed out by symmetry relaxation, and that the resulting smooth topological indicator can be used to design metamaterials. This will be done in the double-SSH model [30], which consists of two coupled, parallel SSH chains [Fig. 3(a)]. In the double-SSH model, the Berry phase is zero for both topological and trivial configurations, hence the need for an alternative topological index. The system is described by the Hamiltonian

$$H_D(k) = \begin{pmatrix} V + \epsilon_1 & t_1 + s_1 e^{ik} & c_v & c_x + c_x e^{ik} \\ t_1 + s_1 e^{-ik} & V - \epsilon_1 & c_x + c_x e^{-ik} & c_v \\ c_v & c_x + c_x e^{ik} & V + \epsilon_2 & t_2 + s_2 e^{ik} \\ c_x + c_x e^{-ik} & c_v & t_2 + s_2 e^{-ik} & V - \epsilon_2 \end{pmatrix}, \quad (6)$$

where  $V$  is a local potential that has the effect of shifting the eigenfrequencies/energies without changing the eigenfunctions,  $t_1$ ,  $t_2$ ,  $s_1$ , and  $s_2$  are the real-valued hopping potentials for the two chains,  $c_x$  and  $c_v$  are the real-valued cross and vertical chain coupling strengths, and  $\epsilon_1$  and  $\epsilon_2$  are real-valued inversion symmetry-breaking terms introduced to obtain a smooth topological indicator.

The topological invariant is defined as  $\nu = n_-(0) - n_-(\pi)$  [29] where  $n_-(k)$  is the number of Bloch eigenfunctions with  $-1$  parity eigenvalue, evaluated at the point  $k$ . In inversion-symmetric systems, the parity eigenfunctions can only take values  $+1$  or  $-1$  at the inversion-symmetric momenta, and the invariant  $\nu$  can be stated as [29,29,43]

$$\nu = \frac{1}{2} \text{Tr}[U^\dagger(0)(\hat{I} - \hat{P})U(0)] - \frac{1}{2} \text{Tr}[U^\dagger(\pi)(\hat{I} - \hat{P})U(\pi)], \quad (7)$$

where  $\hat{I}$  is the identity operator,  $\hat{P}$  is a parity transformation, and  $U(k)$  is a matrix whose columns are the normalized Bloch eigenfunctions below the band gap of interest, evaluated at the momentum point  $k$ . Equation (7) is gauge-invariant and  $\nu$  becomes quantized when the inversion symmetry ( $\epsilon_1 = \epsilon_2 = 0$ ) is respected [Fig. 3(b)].

If we relax the inversion symmetry by setting  $\epsilon_1 \neq 0$  and  $\epsilon_2 \neq 0$ , Eq. (7) becomes a smoothly-varying function [Fig. 3(c)]. Under these conditions,  $\nu$  cannot be interpreted as a topological quantity. However, since  $\nu$  varies smoothly with the system parameters and equals the topological invariant when symmetry is respected, it can be interpreted as a smooth topological indicator and used to guide a search algorithm towards a topological configuration. The search process is illustrated in Fig. 3(c). Figure 3(d) shows the changes in the response of a finite, classical mass-spring implementation [30] as the parameters are changed following the gradient of the smooth topological indicator. At the start of the optimization, both bulk and boundary sites present a band gap, and no in-gap boundary modes are present. As the optimization progresses, modes from the upper and lower bulk bands merge and become increasingly localized at the boundary, finally becoming the expected boundary modes of the double-SSH model. This merging process can be seen to occur twice in Fig. 3(d), as expected from a system composed of two SSH lattices.

Design by symmetry relaxation can also be applied to higher-order topological insulators (HOTIs), systems where the nontrivial bulk topology gives rise to boundary modes that are more than one dimension below that of the bulk [23,24]. Two-dimensional (2D) HOTIs can

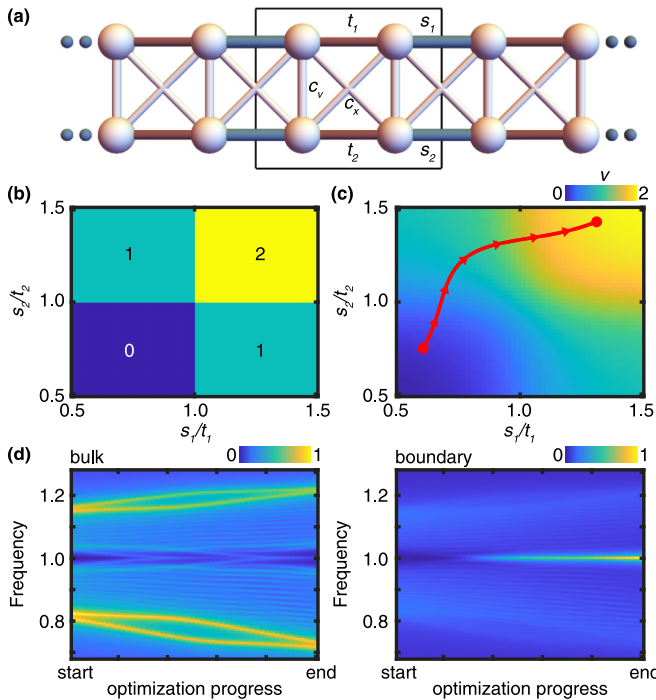


FIG. 3. Relaxation of topological indices based on symmetry eigenvalues at inversion-symmetric momenta. (a) Double-SSH chain with couplings  $t_1$ ,  $t_2$ ,  $s_1$ ,  $s_2$ ,  $c_v$ , and  $c_x$ . (b) Topological index in the presence of inversion symmetry. (c) Topological index after the symmetry has been lifted by perturbations  $\epsilon_i \neq 0$ . The red line represents a gradient-ascending optimization trajectory. (d) Bulk and boundary responsivity  $|\Psi|^2(\omega)$  of a finite sample, as the hopping strengths are being optimized from a trivial to a topological configuration following the red line in (c).

be protected by mirror symmetries  $\mathcal{M}_x$  and  $\mathcal{M}_y$ . For such systems, we introduce a topological characterization [30] based on four mirror-graded invariants [28,29,44] of the form  $v_{\pm}^x = |\theta_{\pm}(k_x = 0) - \theta_{\pm}(k_x = \pi)|$  and  $v_{\pm}^y = |\theta_{\pm}(k_y = 0) - \theta_{\pm}(k_y = \pi)|$ , with the topological phase characterized by  $v_{\pm}^x = v_{\pm}^y = \pi$ . The quantities  $\theta_{\pm}$  are multiband Berry phases calculated on a subset of the bands below the gap of interest, selected according to the band symmetry characteristics, with  $\theta_+$  ( $\theta_-$ ) being the multiband Berry phase calculated using the bands with positive (negative) eigenvalue according to a classifying symmetry. The classifying symmetry will be  $\mathcal{M}_x$  ( $\mathcal{M}_y$ ) when calculating the invariants  $v_{\pm}^x$  ( $v_{\pm}^y$ ). The multiband Berry phases that appear in the expression of  $v_{\pm}^x$  ( $v_{\pm}^y$ ) are quantized by a different mirror symmetry,  $\mathcal{M}_y$  ( $\mathcal{M}_x$ ), as the one used for classification. Therefore, by relaxing one of the symmetries while respecting the other, a pair of invariants becomes a well-defined smooth topological indicator, as the classification is still possible but the resulting Berry phases are no longer quantized.

Smoothed mirror-graded indicators can be used to design HOTIs in a straightforward way. We will demonstrate this in a square lattice with four sites per unit cell [Fig. 4(a)] described by a Hamiltonian of the form

$$H(k_x, k_y) = H_0 + e^{ik_x} H_x + e^{ik_y} H_y + \text{H.c.}, \quad (8)$$

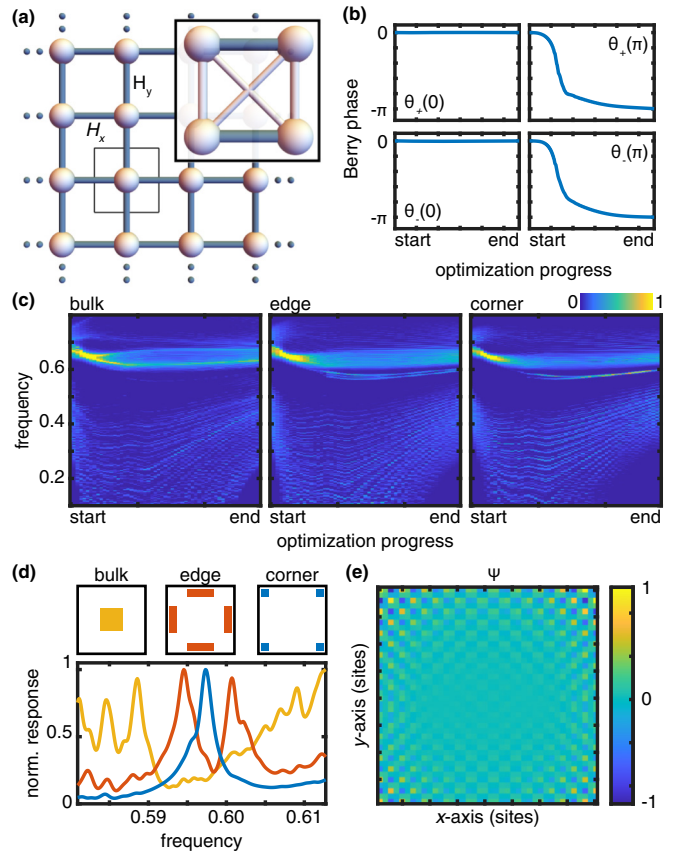


FIG. 4. Symmetry relaxation in higher-order topological insulators. (a) Square lattice with four sites per unit cell (inset). Each unit cell interacts only with nearest-neighbor unit cells. (b) Evolution of the topological invariants  $\theta_{\pm}(k)$  during the design process. (c) Evolution of the frequency spectrum for a finite, classical system consisting of  $20 \times 20$  unit cells, evaluated at the bulk, edges, and corners. (d) Bulk, edge, and corner responsivities  $|\Psi|^2(\omega)$  of the finite classical sample in (c), at the end of the design process. (e) Example of a corner-localized eigenmode of the finite system in (c).

with  $H_0$  representing the potentials and interactions inside the unit cell, and  $H_x, H_y$  the hopping potentials between unit cells in the  $x$  and  $y$  direction, respectively. It should be noted that the model does not require any prior knowledge of higher-order topological systems. It must only be capable of accommodating the appropriate symmetries and provide a search space that is sufficiently large to contain a topological solution.

The optimization process for the invariants  $v_{\pm}^x$  starts from a highly symmetric configuration that respects  $\mathcal{M}_x$ ,  $\mathcal{M}_y$ , and  $\pi/2$ -rotation symmetry  $\mathcal{C}_4$ . During optimization, the classifying symmetry  $\mathcal{M}_x$  is respected, while the quantizing symmetry  $\mathcal{M}_y$  is allowed to relax. The matrices of the system are optimized following a gradient-ascent algorithm, with two additional requirements: First, the direction of change is required to be orthogonal to the gradient of the band gap size, meaning that changes in the system parameters are not allowed to alter the gap size. This is done to prevent the system from undergoing a gap closing during optimization, which could result in an exchange of classifying symmetry eigenvalues. Second, as the optimization progresses,

violations of the  $\mathcal{M}_y$  symmetry are increasingly penalized, as this system does not naturally converge to a symmetric configuration at the end of the optimization. As shown in the Supplemental Material [30], the presence of the  $\mathcal{M}_x$  and  $\mathcal{M}_y$  symmetries causes the topological invariants along  $y$  to be equal to those along  $x$ , and therefore the system ends up in a fully topological configuration. In this example, the optimization process can get trapped in local minima, which we escape by restarting the optimization from a different random configuration (see Supplemental Material for a discussion and source code for the optimization algorithms [30]). For more complex metamaterials, advanced stochastic algorithms such as the Hamiltonian Monte Carlo [45] will be more computationally efficient than simply restarting when trapped on local minima.

The optimization process is illustrated in Figs. 4(b) and 4(c). The four multiband Berry phases converge to quantized values of 0 or  $\pi$  [Fig. 4(b)]. As the optimization progresses, edge and corner modes nucleate [Fig. 4(c)]. The system ends up presenting the hallmarks of higher-order topology [11], namely gapped edge states in the bulk band gap, and corner states in the edge gap [Fig. 4(d)]. The eigenfunction corresponding to one of such eigenstates is presented in Fig. 4(e).

In conclusion, we have demonstrated an approach to efficiently design topological metamaterials. The approach starts by relaxing the symmetries of the model through the addition of symmetry-breaking potential terms. When the symmetries

are relaxed, the topological indicators are no longer quantized. They instead become smooth functions of the system parameters such as hopping strengths, geometric parameters, or stiffness values. We can then use gradient-based methods to efficiently identify the parameter values that result in a topological configuration. This is significant because it provides a universal method for discovering topological phases of parametrized models, where only the topological invariant and relevant symmetries must be known in advance. While we have demonstrated the approach in tight-binding models and phononic metamaterials, the approach is general and therefore provides a route towards the realization of topological phases in diverse platforms such as photonic metamaterials or ultracold atoms. In fact, we expect the approach to be applicable to all symmetry-protected topological systems, including crystalline topological insulators [5] or those protected by chiral, time-reversal, or parity symmetries [4].

The authors would like to thank Valerio Peri, Eliška Greplova, and Sebastian Huber for helpful discussions. This work was supported by the European Research Council (ERC) under the European Union's Horizon 2020 Research and Innovation Programme (Grant Agreements No. 694407 and No. 714069). T.D. acknowledges funding from the ETH Zurich Postdoctoral Fellowship program. F.S. was supported by the Swiss National Science Foundation (Grant No. 200021\_169061).

- 
- [1] K. v. Klitzing, G. Dorda, and M. Pepper, New Method for High-Accuracy Determination of the Fine-Structure Constant Based on Quantized Hall Resistance, *Phys. Rev. Lett.* **45**, 494 (1980).
  - [2] D. J. Thouless, M. Kohmoto, M. Nightingale, and M. den Nijs, Quantized Hall Conductance in a Two-Dimensional Periodic Potential, *Phys. Rev. Lett.* **49**, 405 (1982).
  - [3] Z.-H. Zhu, G. Levy, B. Ludbrook, C. N. Veenstra, J. A. Rosen, R. Comin, D. Wong, P. Dosanjh, A. Ubaldini, P. Syers *et al.*, Rashba Spin-Splitting Control at the Surface of the Topological Insulator  $\text{Bi}_2\text{Se}_3$ , *Phys. Rev. Lett.* **107**, 186405 (2011).
  - [4] S. Ryu, A. P. Schnyder, A. Furusaki, and A. W. Ludwig, Topological insulators and superconductors: Tenfold way and dimensional hierarchy, *New J. Phys.* **12**, 065010 (2010).
  - [5] L. Fu, Topological Crystalline Insulators, *Phys. Rev. Lett.* **106**, 106802 (2011).
  - [6] R.-J. Slager, A. Mesaros, V. Juričić, and J. Zaanen, The space group classification of topological band-insulators, *Nat. Phys.* **9**, 98 (2013).
  - [7] S. H. Mousavi, A. B. Khanikaev, and Z. Wang, Topologically protected elastic waves in phononic metamaterials, *Nat. Commun.* **6**, 8682 (2015).
  - [8] J. Kruthoff, J. de Boer, J. van Wezel, C. L. Kane, and R.-J. Slager, Topological Classification of Crystalline Insulators through Band Structure Combinatorics, *Phys. Rev. X* **7**, 041069 (2017).
  - [9] B. Bradlyn, L. Elcoro, J. Cano, M. G. Vergniory, Z. Wang, C. Felser, M. I. Aroyo, and B. A. Bernevig, Topological quantum chemistry, *Nature (London)* **547**, 298 (2017).
  - [10] K. H. Matlack, M. Serra-Garcia, A. Palermo, S. D. Huber, and C. Daraio, Designing perturbative metamaterials from discrete models, *Nat. Mater.* **17**, 323 (2018).
  - [11] M. Serra-Garcia, V. Peri, R. Süsstrunk, O. R. Bilal, T. Larsen, L. G. Villanueva, and S. D. Huber, Observation of a phononic quadrupole topological insulator, *Nature (London)* **555**, 342 (2018).
  - [12] L. Piloizzi, F. A. Farrelly, G. Marcucci, and C. Conti, Machine learning inverse problem for topological photonics, *Commun. Phys.* **1**, 57 (2018).
  - [13] V. Peano, F. Sapper, and F. Marquardt, Rapid exploration of topological band structures using deep learning, [arXiv:1912.03296](https://arxiv.org/abs/1912.03296).
  - [14] T. Mertz and R. Valentí, Engineering topological phases guided by statistical and machine learning methods, [arXiv:2008.11213](https://arxiv.org/abs/2008.11213).
  - [15] C. He, X. Ni, H. Ge, X.-C. Sun, Y.-B. Chen, M.-H. Lu, X.-P. Liu, and Y.-F. Chen, Acoustic topological insulator and robust one-way sound transport, *Nat. Phys.* **12**, 1124 (2016).
  - [16] R. E. Christiansen, F. Wang, and O. Sigmund, Topological Insulators by Topology Optimization, *Phys. Rev. Lett.* **122**, 234502 (2019).
  - [17] R. E. Christiansen, F. Wang, S. Stobbe, and O. Sigmund, Acoustic and photonic topological insulators by topology optimization, *Proc. SPIE* **11080**, 1108003 (2019).
  - [18] J. I. Väyrynen and G. E. Volovik, Soft topological objects in topological media, *JETP Lett.* **93**, 344 (2011).
  - [19] I. Tanaka, Influence of rotational symmetry breaking on topological insulators, *Ann. Phys.* **396**, 71 (2018).

- [20] W. P. Su, J. R. Schrieffer, and A. J. Heeger, Solitons in Polyacetylene, *Phys. Rev. Lett.* **42**, 1698 (1979).
- [21] D. Vanderbilt, *Berry Phases in Electronic Structure Theory: Electric Polarization, Orbital Magnetization and Topological Insulators* (Cambridge University Press, Cambridge, U.K., 2018).
- [22] L. Fu and C. L. Kane, Topological insulators with inversion symmetry, *Phys. Rev. B* **76**, 045302 (2007).
- [23] F. Schindler, A. M. Cook, M. G. Vergniory, Z. Wang, S. S. P. Parkin, B. A. Bernevig, and T. Neupert, Higher-order topological insulators, *Sci. Adv.* **4**, eaat0346 (2018).
- [24] W. A. Benalcazar, B. A. Bernevig, and T. L. Hughes, Quantized electric multipole insulators, *Science* **357**, 61 (2017).
- [25] W. P. Su, J. R. Schrieffer, and A. J. Heeger, Soliton excitations in polyacetylene, *Phys. Rev. B* **22**, 2099 (1980).
- [26] M. J. Rice and E. J. Mele, Elementary Excitations of a Linearly Conjugated Diatomic Polymer, *Phys. Rev. Lett.* **49**, 1455 (1982).
- [27] B. J. Wieder, Z. Wang, J. Cano, X. Dai, L. M. Schoop, B. Bradlyn, and B. A. Bernevig, Strong and fragile topological Dirac semimetals with higher-order Fermi arcs, *Nat. Commun.* **11**, 627 (2020).
- [28] A. Alexandradinata and B. A. Bernevig, Berry-phase description of topological crystalline insulators, *Phys. Rev. B* **93**, 205104 (2016).
- [29] A. Alexandradinata, X. Dai, and B. A. Bernevig, Wilson-loop characterization of inversion-symmetric topological insulators, *Phys. Rev. B* **89**, 155114 (2014).
- [30] See Supplemental Material at <http://link.aps.org/supplemental/10.1103/PhysRevB.102.241404> for a discussion of the higher-order topological invariant, source codes, and finite element simulations, which includes Refs. [46–48].
- [31] Z. Wang, Y. Chong, J. D. Joannopoulos, and M. Soljačić, Observation of unidirectional backscattering-immune topological electromagnetic states, *Nature (London)* **461**, 772 (2009).
- [32] M. Hafezi, S. Mittal, J. Fan, A. Migdall, and J. M. Taylor, Imaging topological edge states in silicon photonics, *Nat. Photonics* **7**, 1001 (2013).
- [33] A. B. Khanikaev, S. Hossein Mousavi, W.-K. Tse, M. Kargarian, A. H. MacDonald, and G. Shvets, Photonic topological insulators, *Nat. Mater.* **12**, 233 (2013).
- [34] R. Süsstrunk and S. D. Huber, Observation of phononic helical edge states in a mechanical topological insulator, *Science* **349**, 47 (2015).
- [35] J. Ningyuan, C. Owens, A. Sommer, D. Schuster, and J. Simon, Time- and Site-Resolved Dynamics in a Topological Circuit, *Phys. Rev. X* **5**, 021031 (2015).
- [36] V. V. Albert, L. I. Glazman, and L. Jiang, Topological Properties of Linear Circuit Lattices, *Phys. Rev. Lett.* **114**, 173902 (2015).
- [37] V. Peri, Z.-D. Song, M. Serra-Garcia, P. Engeler, R. Queiroz, X. Huang, W. Deng, Z. Liu, B. A. Bernevig, and S. D. Huber, Experimental characterization of fragile topology in an acoustic metamaterial, *Science* **367**, 797 (2020).
- [38] C. W. Peterson, W. A. Benalcazar, T. L. Hughes, and G. Bahl, A quantized microwave quadrupole insulator with topologically protected corner states, *Nature (London)* **555**, 346 (2018).
- [39] V. Peri, M. Serra-Garcia, R. Ilan, and S. D. Huber, Axial-field-induced chiral channels in an acoustic Weyl system, *Nat. Phys.* **15**, 357 (2019).
- [40] H. He, C. Qiu, L. Ye, X. Cai, X. Fan, M. Ke, F. Zhang, and Z. Liu, Topological negative refraction of surface acoustic waves in a Weyl phononic crystal, *Nature (London)* **560**, 61 (2018).
- [41] M. Xiao, Z. Q. Zhang, and C. T. Chan, Surface Impedance and Bulk Band Geometric Phases in One-Dimensional Systems, *Phys. Rev. X* **4**, 021017 (2014).
- [42] Y.-W. Tsai, Y.-T. Wang, P.-G. Luan, and T.-J. Yen, Topological phase transition in a one-dimensional elastic string system, *Crystals* **9**, 313 (2019).
- [43] H. C. Po, A. Vishwanath, and H. Watanabe, Symmetry-based indicators of band topology in the 230 space groups, *Nat. Commun.* **8**, 50 (2017).
- [44] F. Schindler, M. Brzezińska, W. A. Benalcazar, M. Iraola, A. Bouhon, S. S. Tsirkin, M. G. Vergniory, and T. Neupert, Fractional corner charges in spin-orbit coupled crystals, *Phys. Rev. Research* **1**, 033074 (2019).
- [45] L. Gebraad, C. Boehm, and A. Fichtner, Bayesian elastic full-waveform inversion using Hamiltonian Monte Carlo, *J. Geophys. Res.: Solid Earth* **125**, e2019JB018428 (2020).
- [46] W. A. Little, Possibility of synthesizing an organic superconductor, *Phys. Rev.* **134**, A1416 (1964).
- [47] Z.-D. Song, L. Elcoro, and B. A. Bernevig, Twisted bulk-boundary correspondence of fragile topology, *Science* **367**, 794 (2020).
- [48] W. A. Benalcazar, T. Li, and T. L. Hughes, Quantization of fractional corner charge in  $C_n$ -symmetric higher-order topological crystalline insulators, *Phys. Rev. B* **99**, 245151 (2019).